Title

Dual-sectored transurethral ultrasound for thermal treatment of stress urinary incontinence: in silico studies in 3D anatomical models

Journal

Medical & Biological Engineering & Computing, 58(6)

ISSN

1357-5481

Authors

Liu, Dong
Adams, Matthew
Burdette, E Clif
et al.

Publication Date

2020-06-01

DOI

10.1007/s11517-020-02152-6

Peer reviewed

HHS Public Access

Author manuscript

Med Biol Eng Comput. Author manuscript; available in PMC 2021 June 01.

Published in final edited form as:

Med Biol Eng Comput. 2020 June ; 58(6): 1325–1340. doi:10.1007/s11517-020-02152-6.

Dual-sectored Transurethral Ultrasound for Thermal Treatment of Stress Urinary Incontinence: *In Silico* Studies in 3D Anatomical Models

Dong Liu[1], **Matthew Adams**[1], **E Clif Burdette**[2], **Chris J Diederich**[1]

[1]Department of Radiation Oncology, University of California San Francisco, San Francisco, CA, USA

[2]Acoustic MedSystems, Inc, Savoy, IL, USA

Abstract

The purpose of this study is to investigate the feasibility and performance of a stationary, non-focused dual-sectored tubular transurethral ultrasound applicator for thermal exposure of tissue regions adjacent to the urethra for treatment of stress urinary incontinence (SUI) through acoustic and biothermal simulations on 3D anatomical models. Parametric studies in a generalized tissue model over dual-sectored ultrasound applicator configurations (acoustic surface intensities, lateral active acoustic output sector angles, and durations) were performed. Selected configurations and delivery strategies were applied on 3D pelvic anatomical models. Temperature and thermal dose distributions on the target region and surrounding tissues were calculated. Endovaginal cooling was explored as a strategy to mitigate vaginal heating. The dual-75-90° sector transurethral tubular transducer (3.5 mm outer diameter (OD), 14 mm length, 6.5 MHz, 8.8-10.2 W/cm^2) and 2-3 min sonication duration were selected from the parametric study for acoustic and biothermal simulations on anatomical models. The transurethral applicator with two opposing 75-90° active lateral tubular sectors can create two heated volumes for a total of up to 1.8 cm^3 over 60 $EM_{43°C}$, with at least 10mm radial penetration depth, 1.2 mm urethral sparing and no lethal damage to the vagina and adjacent bone (<60 $EM_{43°C}$). Endovaginal cooling can be applied to further reduce the vaginal wall exposure (<15 $EM_{43°C}$). Simulations on 3D anatomical models indicate that dual-sectored transurethral ultrasound applicators can selectively heat pelvic floor tissue lateral to the mid-urethra in short treatment durations, without damaging adjacent vaginal and bone tissues, as a potential alternative treatment option for Stress Urinary Incontinence.

Graphic Abstract

Corresponding author: Chris J Diederich, Chris.Diederich@ucsf.edu.

Conflict of interest

E. Clif Burdette is affiliated with Acoustic MedSystems, which has a commercial interest in interstitial ultrasound technology. No potential conflict of interest was reported by other authors.

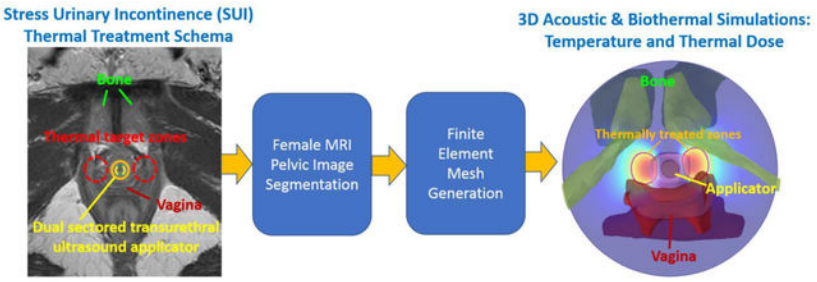

Schema for *in silico* investigation of transurethral ultrasound thermal therapy applicator for minimally invasive treatment of SUI

Keywords

High-intensity ultrasound; therapeutic ultrasound; thermal therapy; simulation; thermal ablation

1. Introduction

Stress Urinary Incontinence (SUI) is the most common type of urinary incontinence disorder suffered by women, which refers to involuntary urine leakage due to physical exertion, sneezing or coughing. It may affect up to 30% of adult women in the US [1,2]. One of the main causes of SUI is attributed to weakening of the endopelvic fascia and supporting tissues near the mid-urethra [3]. Current treatment options include behavior training, absorbent products, occlusive devices, pharmaceutical therapy, surgical procedures and thermal therapy [4-6]. The “gold standard” treatment option is a surgical insertion of synthetic tape in the mid-urethra region, serving as a hammock to support the urethra by increasing sustainable urethral pressure to mitigate unintended urine leakage [7]. However, this procedure requires lengthy anesthetic intervention and can result in complications and prolonged recovery [8,9]. Minimally-invasive alternatives to these surgical procedures and non-surgical options are being investigated as a means to potentially provide a more clinically desirable and durable treatment.

Thermal therapy is a minimally invasive alternative treatment option for SUI, whereby energy-based devices can be inserted and positioned locally and applied to heat pelvic supportive tissues. Moderate thermal exposure can induce tissue damage to produce collagen shortening, shrinkage and neocollagenesis to tighten or remodel target tissues, potentially increasing urethral support [10-12]. The objective of thermal therapy for treatment of SUI is to create large thermally induced damage and subsequent remodeling zones within the supportive pelvic connective tissues while protecting sensitive organs. Transurethral catheter devices, with small deployable RF needles on the distal end, have been applied to deliver energy to the bladder neck region in order to remodel the adjacent supportive tissue, which showed a significant reduction in leakage events and quality of life improvement; in practice this device, due to the short length and small diameter of the deployable RF tines, produces small zones of coagulation and requires multiple positionings and redeployments of the RF needle electrodes through the urethra to extend the coagulation into larger zones [13-15]. Laser devices have also been utilized for thermal treatment of vaginal laxity, pelvic organ

prolapse and restoration of vaginal function [16,17]. Recent studies have investigated the potential of laser energy to thermally coagulate endopelvic connective tissue for treating SUI by a transurethral or transvaginal approach; however, due to the high-power absorption and scattering of photons in the urethral and vaginal mucosa compared to the deeper tissues, the maximum power delivered and thus depth of penetration was limited in order to reduce undesirable thermal damage at the vagina or urethral submucosa [18-20].

In consideration of limitations of other thermal therapy techniques for treatment of SUI, catheter-based ultrasound may offer advantages of deeper energy penetration, specific targeting and spatial control of energy depositions, a flexible delivery catheter for positioning in the urethra, and integrated cooling for protection of non-target regions [21]. As an example, transurethral ultrasound applicator configurations with multi-sectored tubular transducers, as developed for prostate applications, can provide wider and larger angular heated zones without applicator movement [22,23]. In contrast, transurethral ultrasound applicators specific to prostate, with either planar or curvilinear transducers, can generate directional heating from the urethra and be rotated to sweep through tissue targets sequentially, with narrow and deep heating patterns [24-26], and have been applied for the clinical treatment of prostate cancer under MRI guidance [27]. Recently, a transurethral applicator design incorporating a curvilinear focused transducer has been investigated by our group through simulations and shown to heat the supportive tissue near the urethra as a means to potentially treat SUI, albeit with the requirements of sequential rotations and sonications during the procedure to create multiple separate narrow heated zones each of ~15mm penetration while preserving the urethra and vagina. However, in consideration of clinical delivery, this curvilinear focused device would require manipulation and precise orientation of the device during treatment; and its narrow and deep-penetrating non-diverging acoustic beam may be incident on the pelvic bone, which could cause excessive heating on the bone surface [28,29].

As a more practical design that will not require manipulation or movement during the procedure, we are considering the use of a single multi-sectored tubular transducer transurethral applicator, with dual opposing active sectors that each emit angularly directional and diverging acoustic energy patterns to simultaneously heat pelvic supportive tissues on both lateral sides of the urethra, while inactive sectors are positioned to avoid energy deposition into surrounding bone and vagina (Fig. 1). Thus, an objective of this study is to use numerical simulations to investigate design parameters such as active and inactive sector angles, and performance characteristics specific to a multi-sectored transurethral ultrasound applicator for the treatment of SUI, with the intent of generating large sector shaped heating volumes without applicator manipulation as a possible means of engendering tissue remodeling and a thermally induced “hammock” for treatment of SUI. Therefore, 3D acoustic and biothermal simulations were performed in generalized tissue and anatomical models of the female pelvis, and temperature and thermal dose distributions were calculated and analyzed. Parametric studies were performed to assess device performance as a function of the active sector angles of the tubular transducers, applied acoustic powers, and therapy durations. Selected applicator configurations were employed in three patient specific models with different pelvic and vagina structures to bracket intended usage and determine applicator orientation and placement. Enhancement of thermal sparing of sensitive tissues

via implementation of endovaginal cooling was also investigated. The intent of the study is to obtain applicator design and treatment parameters that achieve a thermal exposure suitable for treatment of SUI within short durations (<5 min), for moderate thermal exposure (~50-60°C) on the pelvic supportive tissue around the mid-urethra with large heated volume over 1.5cm^3 (>60 $EM_{43°C}$) and ~10 mm penetration while providing good sparing (<30 $EM_{43°C}$) of sensitive organs, including the urethral mucosa, vagina wall and pubic bones.

2. Methods

2.1 Model of dual-sectored tubular applicator

The applicator design concept modeled here for transurethral ultrasound thermal treatment of SUI (Fig. 2) includes a tubular transducer (3.5 mm OD (outside diameter), 14 mm length, 6.5MHz) with interior air-backing and electrode surface scoring to produce four separate angular sectors – two inactive sectors without power output and two opposing active sectors, each under independent power control [30]. The transducer assembly is positioned at the distal end of a flexible catheter (4mm OD) within an expandable cooling balloon (7 mm OD, 20 mm length, inflated when deployed) filled with circulating water at constant temperature. This basic schema extends upon design principles previously developed for transurethral prostate ablation [22,23,30,31], where more comprehensive details on fabrication methods and device technical details can be found. The transurethral applicator is positioned within the urethra, with the transducer centered approximately 15 mm from the bladder neck, aiming to treat the weakest area of supportive tissue lateral to the mid-urethra [3]. In practice, but not shown, a balloon on the distal tip of the transurethral applicator can be incorporated that once inflated can anchor in the bladder neck to maintain positioning during treatment [22]. For purposes of this simulation study, the angular extent of the two opposing active sectors was set between 75-105°, which includes a 5° acoustic output dead zone on each sector boundary as expected with transducer scoring [22]. The explored angular extent range of the posterior directed or lower inactive sector γ (Fig. 2) was 101-121°, and for the anterior directed upper inactive sector β was 59°-99° based on patient pelvic geometry in order to minimize energy delivery to the vagina and pubic bones. (Fig. 2). Ambient 22°C cooling water in the balloon was adopted to couple the ultrasound energy and cool the transducer and the surface of urethral mucosa.

2.2 Theory

The acoustic power deposition of a tubular ultrasound applicator in a cylindrical coordinate system can be approximated as follows [32,33]:

$$Q = \frac{2\alpha I_0 r_0}{r} e^{-2\int_{r_0}^{r} \mu dr'} \quad (1)$$

where α (Np/m) is the acoustic absorption coefficient of the tissue, I_0 (W/m^2) is the acoustic surface intensity, r_0 (m) is the radius of the transducer, r (m) is the radial distance from the transducer center, and μ is the acoustic amplitude attenuation coefficient (Np/m). We assume all acoustic energy is absorbed locally and that the absorption coefficient is equal to the amplitude attenuation coefficient. The intensity I_0 is applied to the active surface only as

depicted in Fig. 2, and decays radially according to (1). This acoustic modeling approach has been validated against experiments for directional catheter-based devices [22,34].

The transient temperature profiles resulting from the ultrasound energy deposition can be calculated using the Pennes bio-heat equation [35]:

$$\rho C\frac{\partial T}{\partial t} = \nabla \cdot (k\nabla T) - \omega C_b(T - T_b) + Q \tag{2}$$

where ρ (kg/m^3) is the tissue density, C (J·kg^{-1}·K^{-1}) is the specific heat of tissue, k (W·m^{-1}·K^{-1}) is the tissue thermal conductivity, ω (kg·m^{-3}·s^{-1}) is the blood perfusion rate, C_b (J·kg^{-1}·K^{-1}) and T_b (K) denote blood specific heat and blood temperature (37°C), respectively. Q (W/m^3) is the ultrasound power deposition calculated by (1). The contributions due to metabolism are neglected. Convective heat transfer boundary conditions were applied according to the following expression:

$$\overrightarrow{n} \cdot k\nabla T = h(T_\infty - T) \tag{3}$$

where $\overrightarrow{n}$ represents the outward normal vector, h is the convective heat transfer coefficient (W·m^{-2}·K^{-1}) and T_∞ is the cooling water temperature.

Thermal dose exposure is determined from the calculated transient temperature distributions using the Sapareto and Dewey iso-effect thermal dose in terms of equivalent minutes of heating at 43°C ($EM_{43°C}$) [36,37]:

$$EM_{43^\circ C} = \int_0^t R^{43-T}dt, \quad R = \begin{cases} 0.5, & T > 43^\circ C \\ 0.25, & T < 43^\circ C \end{cases} \tag{4}$$

While the extent of thermal damage and thermally induced remodeling varies on different tissue types, a value of 40-80 $EM_{43°C}$ can define a threshold for reversible non-lethal thermal damage for most types of soft tissue, and a value of 240 $EM_{43°C}$ can define a threshold for lethal coagulation or necrosis [38,39]. In this study, we used the values of 30 $EM_{43°C}$, 60 $EM_{43°C}$ and 240 $EM_{43°C}$ to define the threshold of mild exposure, moderate thermal exposure, and thermal coagulation on pelvic tissue.

Acoustic calculations of the power deposition onto the computational mesh were performed in MATLAB 2016b (MathWorks, Natick, MA), and imported into COMSOL Multiphysics 5.2 (COMSOL Inc., Burlington, MA) for corresponding finite element method (FEM)-based temperature and thermal dose calculations. Dirichlet conditions constrained the outer boundaries of the computational domain to 37°C. Cooling of the urethra by water-circulation through the 7 mm OD applicator balloon was modeled using Eq. 3 with h of 1000 W/m^2/K and T_∞ set as 22°C [28,40]. Tissue perfusion was modeled as a dynamic process, with a constant nominal value as listed in Table 1, and reduced to 0 at thermal doses greater than 300 $EM_{43°C}$ [41].

2.3 Parametric study

To characterize the performance of the applicator design and power delivery strategies, parametric studies on treatment configurations (active sector angles, acoustic intensities, applied power, and sonication durations) were performed using a 3D generic tissue model. The generic model (40 mm × 40 mm × 30 mm) assumed homogenous acoustic and biothermal properties (Table 1 [42]). The applicator transducer assembly and water-inflated balloon was positioned in the center depth of the model, at 10 mm from the side. To reduce the computation cost and assuming symmetry, these simulations incorporated a single active sector angle ranging from 75-105°, with the active section facing inward toward the outer 40 mm × 40 mm boundary of the tissue model. Surface intensities ranging from 7.3-11.7 W/cm^2 were applied across active sector angles, with treatment durations of 2-3 min. 1 min pre-sonication water cooling was applied for further protection of urethra, and 2 min of post-sonication time was simulated to incorporate thermal dose accrual during cooling. Two metrics were defined to evaluate the performance: the urethral sparing in radial depth from the balloon boundary, as defined within a thermal dose limit of 30 $EM_{43°C}$; and the penetration depth in terms of radial depth of moderate temperature elevation and thermal insult from the balloon boundary, as defined by the outer extent of the 60 $EM_{43°C}$ thermal dose contour.

Convergence studies were performed on the generic 3D model to determine the appropriate size of the computational domain (radial distances from transducer ranging from 25-45 mm), FEM mesh specifications and transient thermal solver time stepping scheme. As Fig. 3 shows, radial domain extents of 35 mm and 45 mm could generate equivalent temperature elevation within the target thermal zone (<25 mm), indicating that the domain extent of 35 mm was reasonable for accurate thermal solution for temperatures greater than 40°C and reduced computational cost. A varying mesh size scheme was adopted with element dimensions of 0.6 mm, 1.2mm and 2.4 mm within the region of 10 mm, 20 mm and 35 mm radially from the transducer, respectively. As shown in Fig.3b, the temperature results in the central radial line for this mesh is equivalent to the results for a uniform mesh size of 0.5 mm, but with ~70% less computational cost. An implicit time-dependent Backward Differentiation Formula solver (built-in solver in COMSOL Multiphysics) with various time steps (0.1s - 5s) was used in the simulations. Specifically, when sonication was initiated and ended, a series of short time steps (0.1s) were used to force accurate temporal power switching, while at continuous acoustic sonication a constant time step of 5 s was applied. This scheme was compared to a finer variable time-stepping scheme of 0.1-1s, and the absolute maximum temperature discrepancy was less than 0.5°C.

2.4 3D anatomical model generation

To further investigate the performance characteristics of the dual sectored transurethral ultrasound applicators for thermal therapy delivery to pelvic tissue, a total of three separate 3D anatomical models were developed with intent to bracket a range of SUI treatment settings. In general, the mid-urethral anatomy can vary in the shape and proximity of the vaginal wall [43] and in the separation distance of the pelvic bones, which can impact the acoustic deposition and thermal distributions in the lateral target zones. Reviews of anatomical images of the female pelvis indicate typical variations in the shape of the vagina,

which in the majority of cases can be described as “H” shaped, slightly encompassing the urethra, and “M” shaped, flattened and below the urethra [44]. The most relevant anatomy for these simulations is the positioning of the mid-urethra, applicator position, and vagina position and shape, which these variations are now captured across the three cases. The position of the bowel, bladder and uterus will remain outside the thermal treatment domain when considering SUI thermal treatments given that the applicator is always positioned mid-urethra, and is contraindicated for patients with significant pelvic prolapse. Thus, in this study Model I represents a case with a typical “H” shaped vaginal wall and a relatively smaller retropubic space; Model II represents a case with a typical “M” or flattened vaginal wall close to the urethra and relatively larger retropubic space; and Model III represents a clinically challenging case with very limited retropubic space and a flattened vaginal wall structure.

The anatomical models that include the structures of the urethra, vagina, pubic bones and supportive soft tissue regions adjacent to the urethra were segmented from patient pelvic MRI images in Mimics Innovation Suite (Materialise, Leuven, Belgium) as shown in Fig. 4. 3D surfaces of the segmented tissue structures were converted to FEM meshes using 3-Matics (Materialise, Leuven, Belgium). A varying sized mesh was used, as similar to the scheme used in the parametric studies, with element sizes of 0.6, 1.2 and 2.4 mm within radial distances of 10 mm, 20 mm and 40 mm from the applicator and 25% gradual increment between mesh regions.

2.5 Performance studies in 3D anatomical models

Thermal and acoustic properties for each tissue type were applied as shown in Table 1 for acoustic and biothermal modeling [42,45,46]. The acoustic energy was assumed to propagate through the tissue/bone interface with a 65% transmission, based on a previous study of ultrasound-bone interaction using a transurethral ultrasound applicator [28]. Design and treatment parameters selected from the parametric studies were applied to investigate applicator configurations with appropriate upper (or anterior in anatomical perspective) inactive angles for avoiding bone heating and lower (or posterior in anatomical perspective) inactive angles for limiting heating of the vaginal wall. Radial extent of urethral sparing (<30 $EM_{43°C}$) and penetration depth (>60 $EM_{43°C}$), temperature distributions, and iso-temperature and iso-thermal dose volumes were calculated. The maximum temperature and thermal dose in vaginal wall and adjacent bone were also tabulated.

Endovaginal water cooling was also explored as a means of reducing thermal exposure of vaginal tissues during treatment if desired. In practice, this could be accomplished using a water-cooled obturator or balloon inserted within the vaginal cavity during the treatment, as applied in other thermal therapy procedures [24,47]. For these simulations, the vagina was modeled as an isotropic 2.5 mm thick vaginal wall [48] surrounding an inner vaginal lumen filled with cooling fluid. Endovaginal water cooling temperatures of 35°C and 25°C were applied in separate simulations for all three anatomical models, using Eq. 3 and a heat transfer coefficient of 1000 $W/m^2/K$ [40]. Simulations using the 3D anatomical models were performed on a Windows 10 workstation with Dual Intel Xeon CPU E5-2620 v4 2.1GHz

processors and 128 GB RAM. Computational model details and running times for the 3D anatomical models are summarized in Table 2.

3. Results

Simulation results for the parametric studies on the 3D homogenous tissue model over different active sector angles of the tubular transducer are summarized in Fig. 5. For constant acoustic surface intensity, the penetration depth, maximum temperature and heated volume metrics increased while urethral sparing decreased with increasing active sector angles. While different intensity-duration combinations often resulted in similar maximum temperature values and thermal doses, settings with lower intensities and longer durations enhanced the protection of the urethra over higher intensity and shorter duration schemes. Considering applicable treatment configurations for SUI, the applicator with 75-90° active sector angles and surface intensity of 8.8 W/cm^2 for 3 min treatment duration, or 10.2 W/cm^2 for 2 min duration could treat target tissue to a maximum temperature of 54-58°C, with 0.35-0.72 cm^3 heated volume, 9.2-11.0 mm penetration and at least 1.4 mm urethral sparing.

Numerical simulations for the first two anatomical models with normal retropubic space were performed using the dual-sectored tubular applicator with 90° active angles, 8.8W/cm^2 surface intensity (3 W acoustic power to each transducer sector), and 3 min duration. Simulation results for three different applicator configurations with lower inactive angles of 101°, 111° and 121°, are summarized in Table 3 (Model I) and Table 4 (Model II). Due to the limited retropubic space in Model III, simulations were performed to compare the performance of applicator configurations with 75°-90° active angles and treatment settings of 8.8-10.2 W/cm^2 surface intensity and 2-3 min durations. The final temperature and thermal dose maps at the central axial plane, aligned with the mid-urethral target zones, are shown for each model in Fig.6 (Model I), Fig. 7 (a-b), (d-e) (Model II), and Fig. 8 (a-b), (d-e) (Model III). Simulations for Model I and II demonstrated that the dual-90° sectored tubular applicator can simultaneously create two large heated volumes of 1.6-1.8 cm^3 in total over 60 $EM_{43°C}$ directed toward both lateral sides of pelvic tissue adjacent to the urethra, with radial penetrations of 11.1-11.3 mm and heated lengths of 12.5-12.7 mm. The applicator with 121° lower (or posterior directed) inactive sector delivered ultrasound energy to the bone structure and caused moderate thermal damage with a maximum dose of 79.4 $EM_{43°C}$ (Model I, Table 3 and Fig. 6), while the applicator with 101° lower inactive sector resulted in heating of the vaginal wall with a maximum thermal dose of 51.2 $EM_{43°C}$ (Model I, Table 3 and Fig.6). The applicator with 111° lower inactive section could balance the thermal insult on the bone and the vagina, with maximum thermal doses less than 60 $EM_{43°C}$ on both organs. Simulations on Model III demonstrated that the dual-90° sectored tubular applicator could inadvertently generate significant heating of the bone, with small regions of maximum thermal dose over 6000 $EM_{43°C}$ obtained (Model III, Table 5 and Fig.8 (b) and (d)). In contrast, the dual 75° sectored tubular applicator with 8.8-10.2 W/cm^2 and 2-3 min durations resulted in two heated volumes of 0.8-1.1 cm^3 in total over 60 $EM_{43°C}$ on both lateral sides of the urethra, with radial penetration of 9.6-11.3 mm. With a lower inactive sector of 111°, the dual 75° sectored tubular applicator with 2 min sonication could limit thermal exposure to the bone to a maximum dose of 34.8 $EM_{43°C}$, but still generated

moderate heating on the vagina with maximum dose of 85.2 $EM_{43°C}$(Table 5 and Fig.8 (a-b), (d- e)).

Numerical simulations incorporating endovaginal cooling at 35°C and 25°C, using applicators with 101° and 111° lower inactive sectors, were performed and the thermal metrics are summarized for all the anatomical models and compared to non-cooled cases in Tables 3-5. The final temperature and thermal dose maps, as well as the overlays of the 47°C and 60 $EM_{43°C}$ contours at the central axial model planes for the 101° lower inactive sector applicator are shown in (c) and (f) of Fig.7, Fig.8, and Fig.9 for Model I, II, and III, respectively. The simulations on the first two models with normal retropubic space demonstrated that the dual 90° sectored applicator (8.8 W/cm^2, 3 min) combined with endovaginal cooling at 35°C could reduce the thermal insult on the vagina to below the moderate thermal damage threshold (<60 $EM_{43°C}$), whereas 25°C endovaginal cooling could reduce vaginal heating to negligible thermal damage (<10 $EM_{43°C}$). However, endovaginal cooling would also lead to a reduction of the overall therapeutic heated volume, as shown in Table 3 and Table 4. With 35°C and 25°C endovaginal cooling, the heated volumes (>60 $EM_{43°C}$) were 1.4-1.6 cm^3 and 1.0-1.3 cm^3 respectively, correlating to approximately 10% and 30% reduction of the heated volumes obtained without cooling. The reduction of the heated regions and thermal dose exposures in the presence of endovaginal cooling is also demonstrated in the coronal plane along the longitudinal axis of the applicator, with clear reduction of thermal penetration in depth and slight reduction in length across the heated zone, as shown in Fig. 10. Simulations of Model III with limited retropubic space demonstrated that the dual 75° tubular applicator with endovaginal cooling of 25-35°C could significantly reduce the thermal exposure to the vagina from over 80 $EM_{43°C}$ maximum dose to less than 15 $EM_{43°C}$.

A summary of numerical simulation results on models I, II and III, as discussed above along with detailed data shown in Table 3-5, are presented in Fig. 11, using box plots to better illustrate the ranges and differences of urethral sparing, penetrations, volumes, temperature and thermal doses of target organs obtained for the different anatomical models and applicator operating conditions.

4. Discussion

This study investigated design features and performance of a dual-sectored transurethral ultrasound applicator for producing therapeutic temperature distributions in target zones of supportive tissue around the female urethra, with potential for inducing thermal remodeling as a means to treat SUI. The simulation studies demonstrated that the transurethral devices can precisely deliver ultrasound energy through selected active sectors on a tubular transducer, and within a few minutes simultaneously heat target tissue at both lateral sides of the mid-urethra, while providing for protection of urethral submucosa. Further, selection of active sectors and orientations can minimize thermal exposure to the vagina and bone structures. Endovaginal cooling can be applied as a potential strategy to further protect the vaginal wall from thermal insult.

Transurethral ultrasound applicators with multi-sectored tubular transducers provide collimated and directional ultrasound energy output patterns, and through independent activation control of transducer segments can provide spatial control and tailoring of thermal therapy delivery capable of selective treatment of target tissues from within the urethra. Similar applicator configurations have been validated for prostate cancer and benign prostatic hyperplasia (BPH) treatment, demonstrating angular and longitudinal control of acoustic energy into target prostate tissue under MRI or ultrasound guidance, while preserving the urethra by temperature controlled water cooling[22,23,31,49]. As specific for SUI treatment, we investigated a transurethral applicator configuration based upon a tubular transducer with opposing dual-active sectors, to be positioned within the female urethra to allow shaped acoustic energy and therapeutic temperature elevations into targeted supportive tissues. The precise localization and enhanced penetration afforded by ultrasound produces thermal exposure in regions lateral to and immediately adjacent to the mid-urethra, where subsequent remodeling and stiffening may enhance urethral support [18,29]. With dual opposing 90° active sectors, the transurethral applicator can deliver ultrasound energy into two separate wide angular sectored regions. At a nominal applied power of 8.8 W/cm^2 for 3 min duration with 22°C cooling, ~70° directional coverage each on opposite sides of the urethra could be delivered to heat a total volume of target tissue up to 1.8 cm^3 (>60 $EM_{43°C}$), and provide at least 10 mm radial penetration (>60 $EM_{43°C}$) while sparing at least 1.2 mm urethral mucosa. In sharp contrast, current RF and laser treatment are limited in energy penetration and treatment volume, typically 1-5 mm treatment penetration depth from the source, and with 0.6-1.0 mm urethral sparing [13,18-20]. Thus, these numerical simulation results demonstrated that the applicator should provide more spatial control and deeper penetration than current SUI thermal treatments.

Through proper selection of active angles and respective orientation of the dual-sectors and inactive zones, thermal damage to the bone and vagina can be avoided without limitation to the therapeutic temperature elevations and thermal dose delivered to targeted tissues adjacent to the mid-urethra. This simulation study explored varying upper inactive sector angles on 3D anatomical models and demonstrated that with 69° and 79° inactive upper sectors, the transurethral tubular applicator caused negligible thermal exposure (<30 $EM_{43°C}$) to the bones. This low level compares favorably to the more significant levels of bone heating produced using a transurethral curvilinear ultrasound applicator with rotation, although the penetration depth from the urethra for the dual-sectored approach is less [29]. Flattened and H shaped vagina represent the typical variation in patient anatomy and encroachment to the urethra which brackets the range to consider in defining target heating profiles and avoidance patterns [50]. The simulation results demonstrated that the transurethral tubular applicator with 111° lower or posteriorly directed inactive sectors (69° upper or anterior directed inactive sectors correspondingly) can avoid overheating vagina tissue without thermal damage (<60 $EM_{43°C}$) for the first two anatomical models with normal retropubic space considered herein, even without inclusion of endovaginal cooling. Further work can apply pre-treatment imaging across a broader set of prospective patient anatomies with endocavity ultrasound or MRI to inform the patient-specific selection of active angles for maximizing the energy delivery into target regions, and anterior and posterior directed inactive angles for minimizing thermal exposure on the bone and vagina.

This study investigated endovaginal cooling as a means to reduce thermal exposure to the vaginal wall, most notably in cases where the vagina is closely adjacent to the heated regions. Endocavity cooling has been utilized as an efficient safety strategy for protecting sensitive organs, such as endorectal cooling during ultrasound treatment for prostate cancer [24,51,52] and endovaginal cooling during laser SUI treatment [18]. Two endovaginal cooling temperatures were evaluated: 35°C, which represents a more comfortable and easier to tolerate option, could reduce thermal exposure on the vaginal wall with thermal doses less than 60 $EM_{43°C}$ in the models simulated herein; whereas 25°C cooling could reduce the thermal exposure on vagina with maximum thermal doses less than 15 $EM_{43°C}$ on all the models of this study. Lower cooling water temperature might provide more protection of the vaginal wall; however, it could also reduce the total heated volume depending on the proximity of the vagina to the heated tissue regions. Further, in this study a constant 2.5 mm vaginal wall thickness was assumed, based on the average thickness measurements reported in literature [48]. However, a variation in vaginal wall thickness may slightly impact the effect of cooling. It may be possible to assess vaginal wall thickness and target localization *a priori* based upon pretreatment ultrasound imaging, and personalize therapy parameters accordingly for each patient. The selection of cooling temperature would also be dependent on distance of vagina from the applicator, the active sector angles, desired target depth and volume, and patient tolerance to cooling. Future studies could investigate small obturators with cooling that can be positioned within the anterior vagina as means to localize the cooling in regions close to the urethra, and to possibly displace or flatten the vagina to further enhance safety.

These simulation results on 3D pelvic anatomical models provide preliminary treatment guidance and may inform new device development for SUI treatment. We selected a constant frequency (6.5MHz) based on similar applicator configurations for prostate applications[21] and did not consider other frequency ranges. It is likely that lower frequency may increase penetration, heated volumes and urethral sparing, however it may require higher energy input to achieve the same heated volume, and it may also increase the risk of bone heating [28]. We selected the acoustic surface intensities (8.8-10.2 W/cm^2) to each transducer and sonication duration (2-3 min) from parametric studies in order to achieve a short and moderate thermal temperature (50-58°C) and thermal dose (>60 $EM_{43°C}$) exposure on the tissue around the urethra. However, the powers and durations may also vary on different patient cases based on anatomy or be varied and increased during dose finding clinical studies. For instance, some literature reported higher temperature (60-70°) can be explored to produce more significant collagen generation, tightening, and tissue stiffening for SUI treatment [53,54]. Higher powers and longer durations may be needed to achieve this range, and it has been shown to be within the delivery capacity of the transurethral devices [23]. However, application of higher power levels will likely require chilled or lower temperature urethral cooling in order to adequately protect the urethral mucosa. The female urethra is a multi-layer structure of mucosa, submucosa, smooth muscle and striated muscle with a total radial thickness of 2.4-2.8 mm [55], as recorded for the non-distended case, and would likely be thinned during insertion and expansion of a urethral cooling balloon. The treatment configurations discussed above provided at least 1.2 mm urethral sparing (<30 $EM_{43°C}$) to protect the inner layers of urethral mucosa and submucosa

(typically 1.2mm radial thickness [56]), while possibly heating portions of the outermost layers of urethra-striated muscle; portions of the striated muscle zones may provide a viable clinical target for tissue stiffening, as these layers were reported to be weakened in patients with SUI [57]. Based upon this initial *in silico* study, transurethral devices with multi-sectored tubular transducers can be fabricated specific to this application and following the designs herein, applying fabrication techniques similar to those used for image-guided therapy of prostate and cervix [22,23,31,58,59]. Further improvements to the anatomical modeling workflow and numerical implementation may be necessary for real-time treatment planning. Through thermal dosimetry and histological studies in large animals the optimal delivery strategy, with dose ranging (time and power levels) and specific remodeling effects, can be defined and expanded upon based off our studies. Ultimately through clinical implementation and inclusion of dose finding studies, will the clinical efficacy and practicality of this minimally-invasive procedure be established for treatment of SUI.

5. Conclusion

In summary, we performed an *in silico* study to investigate the feasibility and performance of a dual-sectored transurethral ultrasound applicator for delivering therapeutic heating capable of inducing thermal remodeling of pelvic supportive tissue as a potential treatment option for SUI. Multi-sectored tubular transducers with dual active sectors can create two large angular heated volumes on both lateral sides of the tissue adjacent to the urethra, while anterior and posterior directed inactivate sectors can provide protection of the pubic bones and the vagina. Endovaginal cooling can reduce thermal exposure on the vagina, as a potential strategy during SUI treatment.

Acknowledgement

This work is a collaboration between the University of California, San Francisco and Acoustic MedSystems supported by a Small Business Industry Research grant from the U.S. National Institutes of Health.

Funding

This work was supported in part by the U.S. National Institute of health under Grants R44DK108458 and R44CA121740.

Author Biography

Dong Liu is a postdoctoral scholar in the Thermal Therapy Research Group at the University of California, San Francisco. His research interests include thermal therapy and ablation, computer simulation, therapeutic ultrasound.

Matthew Adams is a research specialist in the Thermal Therapy Research Group at the University of California, San Francisco with research interests in therapeutic ultrasound, thermal therapy, and computational modeling.

Everette C. Burdette, PhD, is President/CEO of Acoustic MedSystems, Inc., a company dedicated to image-guided medical interventions and localized therapies for cancer and benign diseases. Dr. Burdette is an innovator of image-guided cancer management methods and was principal scientist in developing the first intraoperative dosimetry and image

guidance system for radiation implants. He was a faculty member at the University of Illinois at Urbana-Champaign, Emory University School of Medicine, and Georgia Tech. He has worked in radiation oncology, thermal therapy, ultrasound imaging, and urological fields for 40 years and prior to that worked in the development of radar systems and microwave devices for military applications for 7 years.

Chris J. Diederich, PhD, is a Professor in Radiation Oncology and Director of the Thermal Therapy Research Group at the University of California, San Francisco. His research interests are in therapeutic ultrasound, hyperthermia therapy, and thermal ablation with an emphasis on the development of minimally-invasive ultrasound technology and corresponding treatment delivery strategies and planning.

References

1. Dmochowski RR, Blaivas JM, Gormley EA, Juma S, Karram MM, Lightner DJ, Luber KM, Rovner ES, Staskin DR, Winters JC (2010) Update of AUA guideline on the surgical management of female stress urinary incontinence. The Journal of urology 183:1906–1914 [PubMed: 20303102]
2. Abrams P, Cardozo L, Fall M, Griffiths D, Rosier P, Ulmsten U, van Kerrebroeck P, Victor A, Wein A (2002) The standardisation of terminology of lower urinary tract function: report from the Standardisation Sub-committee of the International Continence Society. American journal of obstetrics and gynecology 187:116–126 [PubMed: 12114899]
3. DeLancey JO (1994) Structural support of the urethra as it relates to stress urinary incontinence: the hammock hypothesis. American journal of obstetrics and gynecology 170:1713–1723 [PubMed: 8203431]
4. Davila GW (2011) Nonsurgical outpatient therapies for the management of female stress urinary incontinence: long-term effectiveness and durability. Advances in urology 2011:176498 [PubMed: 21738529]
5. Rovner ES, Wein AJ (2004) Treatment options for stress urinary incontinence. Reviews in urology 6:S29
6. Capobianco G, Madonia M, Morelli S, Dessole F, De Vita D, Cherchi PL, Dessole S (2018) Management of female stress urinary incontinence: a care pathway and update. Maturitas 109:32–38 [PubMed: 29452779]
7. Serati M, Salvatore S, Uccella S, Artibani W, Novara G, Cardozo L, Bolis P (2009) Surgical treatment for female stress urinary incontinence: what is the gold-standard procedure? International Urogynecology Journal 20:619–621
8. Abouassaly R, Steinberg JR, Lemieux M, Marois C, Gilchrist LI, Bourque JL, Tu LM, Corcos J (2004) Complications of tension-free vaginal tape surgery: a multi-institutional review. BJU international 94:110–113 [PubMed: 15217442]
9. Deng DY, Rutman M, Raz S, Rodriguez LV (2007) Presentation and management of major complications of midurethral slings: Are complications under-reported? Neurourology and urodynamics 26:46–52 [PubMed: 17149713]
10. Wall MS, Deng X-H, Torzilli PA, Doty SB, O'Brien SJ, Warren RF (1999) Thermal modification of collagen. Journal of Shoulder and Elbow Surgery 8:339–344 [PubMed: 10472007]
11. Hantash BM, Ubeid AA, Chang H, Kafi R, Renton B (2009) Bipolar fractional radiofrequency treatment induces neoelastogenesis and neocollagenesis. Lasers in surgery and medicine 41:1–9 [PubMed: 19143021]
12. Naseef GS, Foster TE, Trauner K, Solhpour S, Anderson RR, Zarins B (1997) The thermal properties of bovine joint capsule: the basic science of laser-and radiofrequency-induced capsular shrinkage. The American journal of sports medicine 25:670–674 [PubMed: 9302474]
13. Edelstein PS (2006) A preclinical study of nonsurgical radiofrequency collagen remodeling for the treatment of stress urinary incontinence. Expert review of medical devices 3:743–748 [PubMed: 17280538]

14. Elser DM, Mitchell GK, Miklos JR, Nickell KG, Cline K, Winkler H, Wells WG (2009) Nonsurgical transurethral collagen denaturation for stress urinary incontinence in women: 12-month results from a prospective long-term study. Journal of Minimally Invasive Gynecology 16:56–62 [PubMed: 19013110]
15. Crivellaro S, Smith JJ (2009) Minimally invasive therapies for female stress urinary incontinence: the current status of bioinjectables/new devices (adjustable continence therapy, urethral submucosal collagen denaturation by radiofrequency). The Scientific World Journal 9:466–478 [PubMed: 19526186]
16. Vizintin Z, Lukac M, Kazic M, Tettamanti M (2015) Erbium laser in gynecology. Climacteric 18:4–8 [PubMed: 26366793]
17. Gambacciani M, Palacios S (2017) Laser therapy for the restoration of vaginal function. Maturitas 99:10–15 [PubMed: 28364861]
18. Hardy LA, Chang CH, Myers EM, Kennelly MJ, Fried NM (2017) Computer simulations of thermal tissue remodeling during transvaginal and transurethral laser treatment of female stress urinary incontinence. Lasers in surgery and medicine 49:198–205 [PubMed: 26900038]
19. Chang C-H, Myers EM, Kennelly MJ, Fried NM (2017) Optical clearing of vaginal tissues, ex vivo, for minimally invasive laser treatment of female stress urinary incontinence. Journal of Biomedical Optics 22:018002
20. Pardo JI, Solà VR, Morales AA (2016) Treatment of female stress urinary incontinence with Erbium-YAG laser in non-ablative mode. European Journal of Obstetrics & Gynecology and Reproductive Biology 204:1–4 [PubMed: 27448169]
21. Salgaonkar VA, Diederich CJ (2015) Catheter-based ultrasound technology for image-guided thermal therapy: Current technology and applications. International Journal of Hyperthermia 31:203–215 [PubMed: 25799287]
22. Kinsey AM, Diederich CJ, Rieke V, Nau WH, Pauly KB, Bouley D, Sommer G (2008) Transurethral ultrasound applicators with dynamic multi-sector control for prostate thermal therapy: In vivo evaluation under MR guidance. Medical physics 35:2081–2093 [PubMed: 18561684]
23. Sommer G, Pauly KB, Holbrook A, Plata J, Daniel B, Bouley D, Gill H, Prakash P, Salgaonkar V, Jones P, Diederich C (2013) Applicators for magnetic resonance-guided ultrasonic ablation of benign prostatic hyperplasia. Investigative radiology 48:387–394. doi:10.1097/RLI.0b013e31827fe91e
24. Chopra R, Burtnyk M, Haider MA, Bronskill MJ (2005) Method for MRI-guided conformal thermal therapy of prostate with planar transurethral ultrasound heating applicators. Physics in medicine and biology 50:4957 [PubMed: 16237234]
25. Burtnyk M, Chopra R, Bronskill M (2010) Simulation study on the heating of the surrounding anatomy during transurethral ultrasound prostate therapy: A 3D theoretical analysis of patient safety. Medical physics 37:2862–2875 [PubMed: 20632598]
26. Ross AB, Diederich CJ, Nau WH, Rieke V, Butts RK, Sommer G, Gill H, Bouley DM (2005) Curvilinear transurethral ultrasound applicator for selective prostate thermal therapy. Medical physics 32:1555–1565 [PubMed: 16013714]
27. Chin JL, Billia M, Relle J, Roethke MC, Popeneciu IV, Kuru TH, Hatiboglu G, Mueller-Wolf MB, Motsch J, Romagnoli C (2016) Magnetic Resonance Imaging–Guided Transurethral Ultrasound Ablation of Prostate Tissue in Patients with Localized Prostate Cancer: A Prospective Phase 1 Clinical Trial. European urology 70:447–455 [PubMed: 26777228]
28. Wootton JH, Ross AB, Diederich CJ (2007) Prostate thermal therapy with high intensity transurethral ultrasound: The impact of pelvic bone heating on treatment delivery. International journal of hyperthermia 23:609–622 [PubMed: 18097849]
29. Liu D, Adams MS, Burdette EC, Diederich CJ (2018) Transurethral high-intensity ultrasound for treatment of stress urinary incontinence (SUI): simulation studies with patient-specific models. International Journal of Hyperthermia 34:1236–1247 [PubMed: 29566562]
30. Burdette EC, Lichtenstiger C, Rund L, Keralapura M, Gossett C, Stahlhut R, Neubauer P, Komadina B, Williams E, Alix C Ultrasound therapy applicators for controlled thermal modification of tissue. In: Proc. of SPIE Vol, 2011 pp 79010W–79011

31. Diederich C, Stafford R, Nau W, Burdette E, Price R, Hazle J (2004) Transurethral ultrasound applicators with directional heating patterns for prostate thermal therapy: in vivo evaluation using magnetic resonance thermometry. Medical Physics 31:405–413 [PubMed: 15000627]
32. Diederich C, Burdette E (1996) Transurethral ultrasound array for prostate thermal therapy: initial studies. IEEE transactions on ultrasonics, ferroelectrics, and frequency control 43:1011–1022
33. Diederich CJ, Hynynen K (1989) Induction of hyperthermia using an intracavitary multielement ultrasonic applicator. IEEE Transactions on Biomedical Engineering 36:432–438 [PubMed: 2714822]
34. Tyréus PD, Diederich CJ (2002) Theoretical model of internally cooled interstitial ultrasound applicators for thermal therapy. Physics in Medicine & Biology 47:1073 [PubMed: 11996056]
35. Pennes HH (1948) Analysis of tissue and arterial blood temperatures in the resting human forearm. Journal of applied physiology 1:93–122 [PubMed: 18887578]
36. Sapareto SA, Dewey WC (1984) Thermal dose determination in cancer therapy. International Journal of Radiation Oncology* Biology* Physics 10:787–800
37. Dewey WC (2009) Arrhenius relationships from the molecule and cell to the clinic. International journal of hyperthermia 25:3–20 [PubMed: 19219695]
38. Yarmolenko PS, Moon EJ, Landon C, Manzoor A, Hochman DW, Viglianti BL, Dewhirst MW (2011) Thresholds for thermal damage to normal tissues: an update. International Journal of Hyperthermia 27:320–343 [PubMed: 21591897]
39. McDannold N, Tempany CM, Fennessy FM, So MJ, Rybicki FJ, Stewart EA, Jolesz FA, Hynynen K (2006) Uterine leiomyomas: MR imaging–based thermometry and thermal dosimetry during focused ultrasound thermal ablation. Radiology 240:263–272 [PubMed: 16793983]
40. Wootton JH, Prakash P, Hsu I-CJ, Diederich CJ (2011) Implant strategies for endocervical and interstitial ultrasound hyperthermia adjunct to HDR brachytherapy for the treatment of cervical cancer. Physics in Medicine & Biology 56:3967 [PubMed: 21666290]
41. Prakash P, Diederich CJ (2012) Considerations for theoretical modelling of thermal ablation with catheter-based ultrasonic sources: Implications for treatment planning, monitoring and control. International journal of hyperthermia 28:69–86 [PubMed: 22235787]
42. Duck FA (2013) Physical properties of tissues: a comprehensive reference book. Academic press,
43. Strohbehn K, Quint LE, Prince MR, Wojno KJ, Delancey JO (1996) Magnetic resonance imaging anatomy of the female urethra: a direct histologic comparison. Obstetrics & Gynecology 88:750–756 [PubMed: 8885907]
44. Tillack AA, Joe BN, Yeh BM, Jun SL, Kornak J, Zhao S, Deng D (2015) Vaginal shape at resting pelvic MRI: predictor of pelvic floor weakness? Clinical imaging 39:285–288 [PubMed: 25457574]
45. Mcintosh RL, Anderson V (2010) A comprehensive tissue properties database provided for the thermal assessment of a human at rest. Biophysical Reviews and Letters 5:129–151
46. Hasgall P, Di Gennaro F, Baumgartner C, Neufeld E, Lloyd B, Gosselin M, Payne D, Klingenböck A, Kuster N (2018) IT'IS Database for thermal and electromagnetic parameters of biological tissues. Version 4.0, May 15, 2018. doi: 10.13099. VFP21000-04-0.* Onl: www. itis. ethz. ch/database,
47. Nau W, Diederich C, Ross A, Rieke V, Butts K, Sommers G Evaluation of endorectal and urethral cooling devices during MR-guided ultrasound thermal ablation in canine prostate In: Engineering in Medicine and Biology Society, 2004. IEMBS'04. 26th Annual International Conference of the IEEE, 2004. IEEE, pp 2492–2495
48. Lara LADS Da Silva AR, Rosa-e-Silva JC, Chaud F, Silva-de-Sá MF, e Silva ARM, Rosa ACJDS (2009) Menopause leading to increased vaginal wall thickness in women with genital prolapse: Impact on sexual response. The journal of sexual medicine 6:3097–3110 [PubMed: 19656272]
49. Hazle JD, Diederich CJ, Kangasniemi M, Price RE, Olsson LE, Stafford RJ (2002) MRI-guided thermal therapy of transplanted tumors in the canine prostate using a directional transurethral ultrasound applicator. Journal of Magnetic Resonance Imaging 15:409–417 [PubMed: 11948830]
50. Fielding JR, Dumanli H, Schreyer AG, Okuda S, Gering DT, Zou KH, Kikinis R, Jolesz FA (2000) MR-based three-dimensional modeling of the normal pelvic floor in women: quantification of muscle mass. American Journal of Roentgenology 174:657–660 [PubMed: 10701604]

51. Burtnyk M, Chopra R, Bronskill MJ (2009) Quantitative analysis of 3-D conformal MRI-guided transurethral ultrasound therapy of the prostate: Theoretical simulations. International Journal of Hyperthermia 25:116–131 [PubMed: 19337912]
52. Diederich C, Nau W, Ross A, Tyreus P, Butts K, Rieke V, Sommer G (2004) Catheter-based ultrasound applicators for selective thermal ablation: progress towards MRI-guided applications in prostate. International journal of hyperthermia 20:739–756 [PubMed: 15675669]
53. Kozma B, Candiotti K, Póka R, Takács P (2018) The Effects of Heat Exposure on Vaginal Smooth Muscle Cells: Elastin and Collagen Production. Gynecologic and obstetric investigation 83:247–251 [PubMed: 29402781]
54. Fistonić N, Fistonić I, Guštek ŠF, Turina ISB, Marton I, Vižintin Z, Kažič M, Hreljac I, Perhavec T, Lukač M (2016) Minimally invasive, non-ablative Er: YAG laser treatment of stress urinary incontinence in women—a pilot study. Lasers in medical science 31:635–643 [PubMed: 26861984]
55. Wieczorek A, Wozniak M, Stankiewicz A, Santoro G, Bogusiewicz M, Rechberger T (2012) 3-D high-frequency endovaginal ultrasound of female urethral complex and assessment of inter-observer reliability. European journal of radiology 81:e7–e12 [PubMed: 20970275]
56. Perucchini D, DeLancey JO, Ashton-Miller JA, Galecki A, Schaer GN (2002) Age effects on urethral striated muscle II. Anatomic location of muscle loss. American journal of obstetrics and gynecology 186:356–360 [PubMed: 11904591]
57. Kim JK, Kim YJ, Choo MS, Cho K-S (2003) The urethra and its supporting structures in women with stress urinary incontinence: MR imaging using an endovaginal coil. American Journal of Roentgenology 180:1037–1044 [PubMed: 12646452]
58. Wootton JH, Hsu I, Joe C, Diederich CJ (2011) Endocervical ultrasound applicator for integrated hyperthermia and HDR brachytherapy in the treatment of locally advanced cervical carcinoma. Medical physics 38:598–611 [PubMed: 21452697]
59. Diederich CJ, Wootton J, Prakash P, Salgaonkar V, Juang T, Scott S, Chen X, Cunha A, Pouliot J, Hsu I Catheter-based ultrasound hyperthermia with HDR brachytherapy for treatment of locally advanced cancer of the prostate and cervix. In: Energy-based Treatment of Tissue and Assessment VI, 2011. International Society for Optics and Photonics, p 79010O

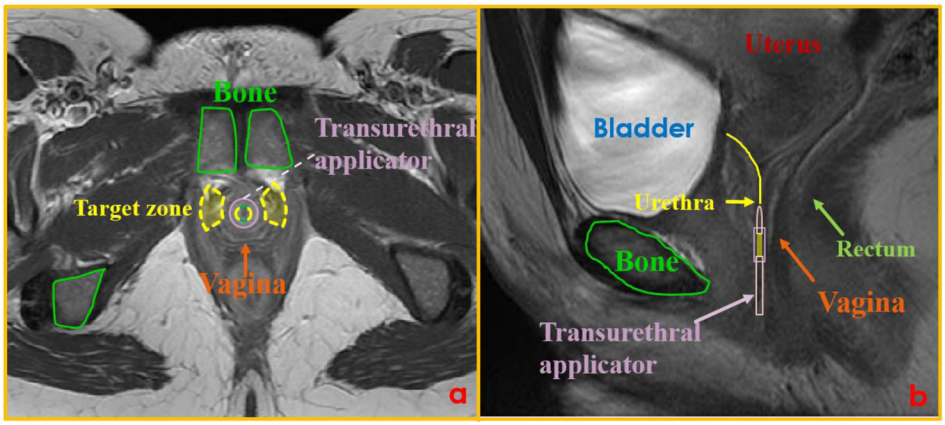

Fig. 1.

A schema of the proposed SUI treatment strategy using a transurethral ultrasound applicator with a multi-sector tubular transducer positioned within the mid-urethra. The tubular transducer is sectored to provide angular patterns of energy deposition with acoustic energy emitted simultaneously from two separate active sectors towards target zones of supportive connective tissue (shown in yellow (a)) on both lateral sides of the mid-urethra, while inactive sectors are directed toward bone and vaginal tissues. The device remains stationary without the need for manipulation during the treatment.

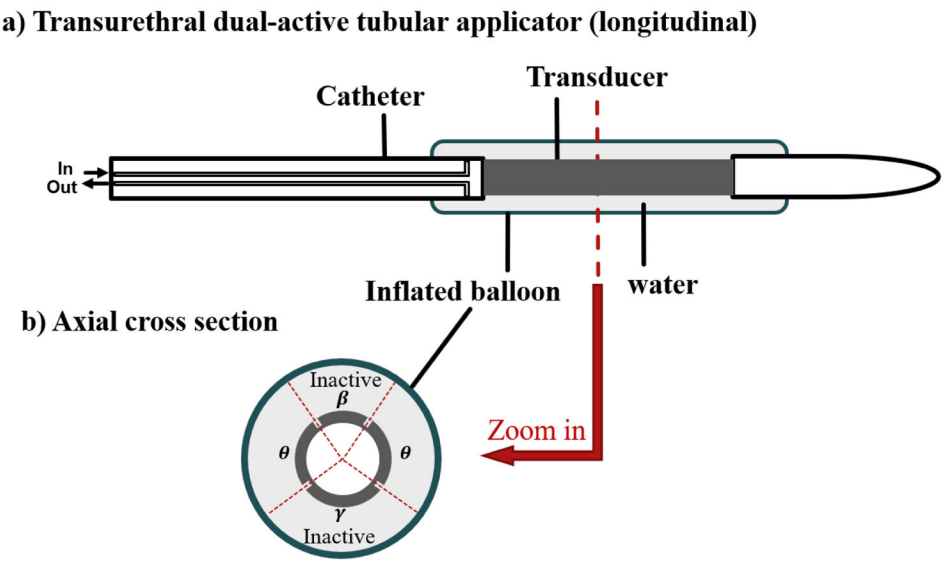

Fig. 2.

The schema of the transurethral applicator in longitudinal (a) and axial cross-sections (b). The multi-sectored tubular transducer includes two active sectors extending down the length of the tube, each with active angle θ for delivering ultrasound energy divergently through lateral sides of the urethra to the target tissue, and two inactive sectors (β and γ) without energy output for protection of bone and vagina tissues.

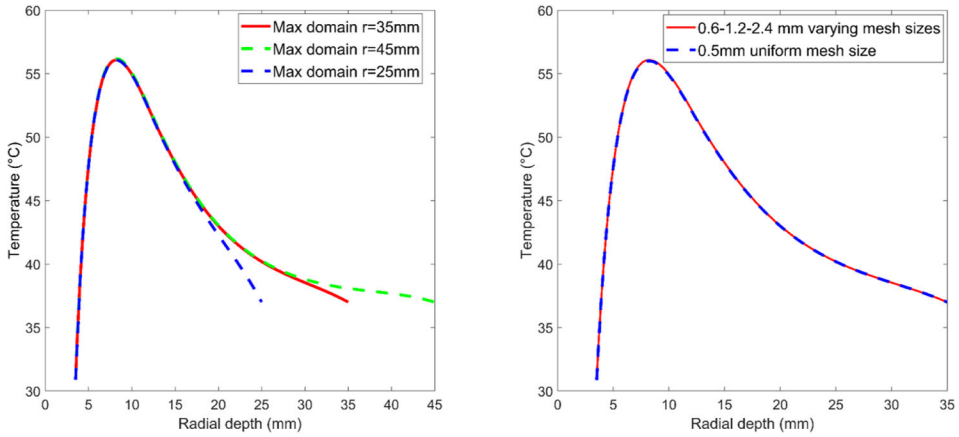

Fig.3.

Convergence study on domain sizes and mesh sizes with the generic model: temperature elevation is shown along the central line radial from the transducer center, with 25 mm, 35 mm, and 45 mm computational domain dimension sizes in radial direction (left), and with constant or varying mesh sizes for the fixed 35 mm radial domain size (right). Maximum domain dimensions of 35-40 mm and the varying mesh size schema were applied in the remainder of the study.

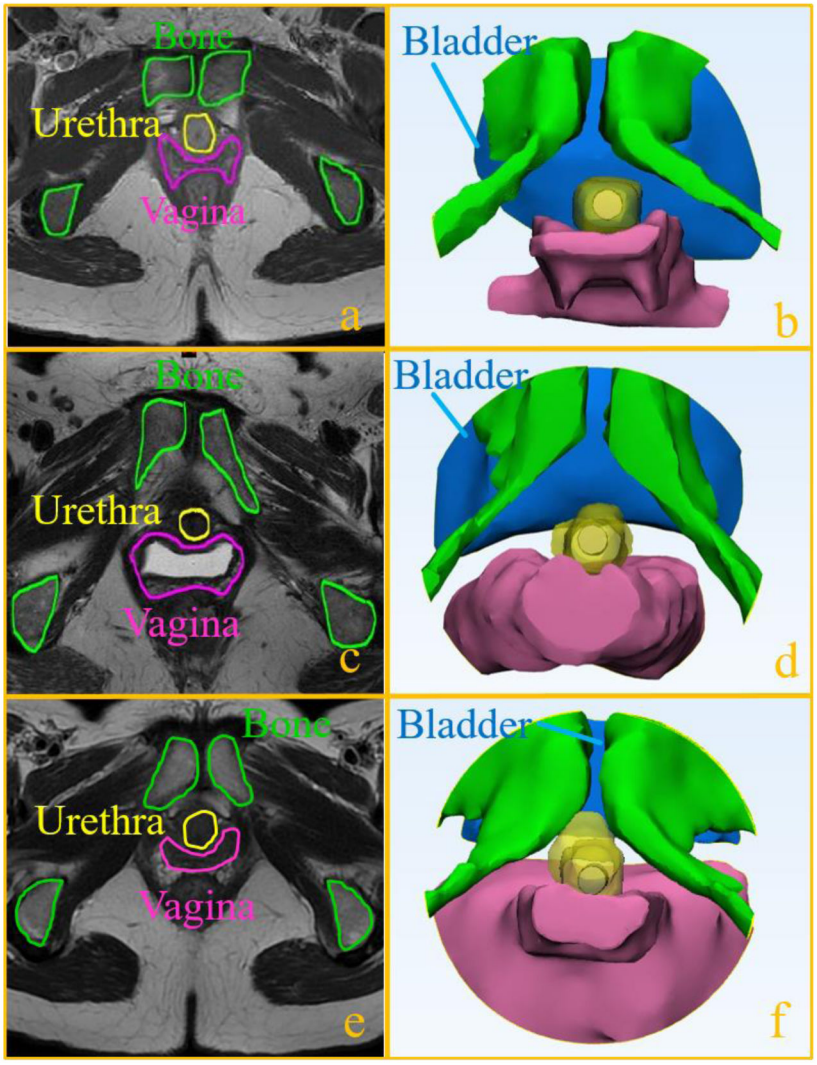

Fig. 4.

The Pelvic MRI images, segmentations and corresponding 3D anatomic models representing three hypothetical SUI cases: Model I with “H” shaped vagina and relatively smaller retropubic space(a and b); Model II with flattened vagina and relatively larger retropubic space (c and d); and Model III with very limited retropubic space and flattened vagina (e and f).

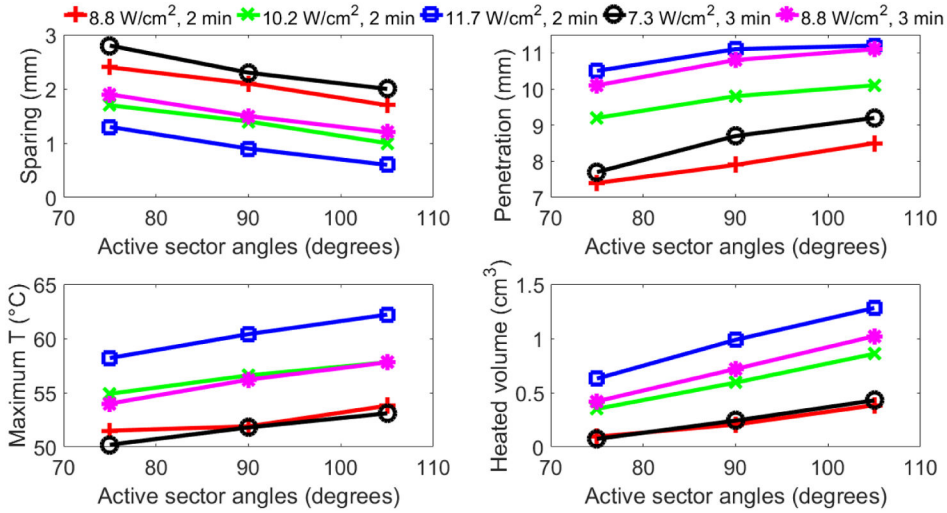

Fig. 5.

Summary of parametric studies on active sector angles: the urethral sparing (<30 $EM_{43°C}$), radial penetration (>60 $EM_{43°C}$), maximum temperature and heated volume (>60 $EM_{43°C}$) at varying acoustic surface intensities (7.3 W/cm^2 -11.7 W/cm^2) of the applicator and sonication durations (2-3min).

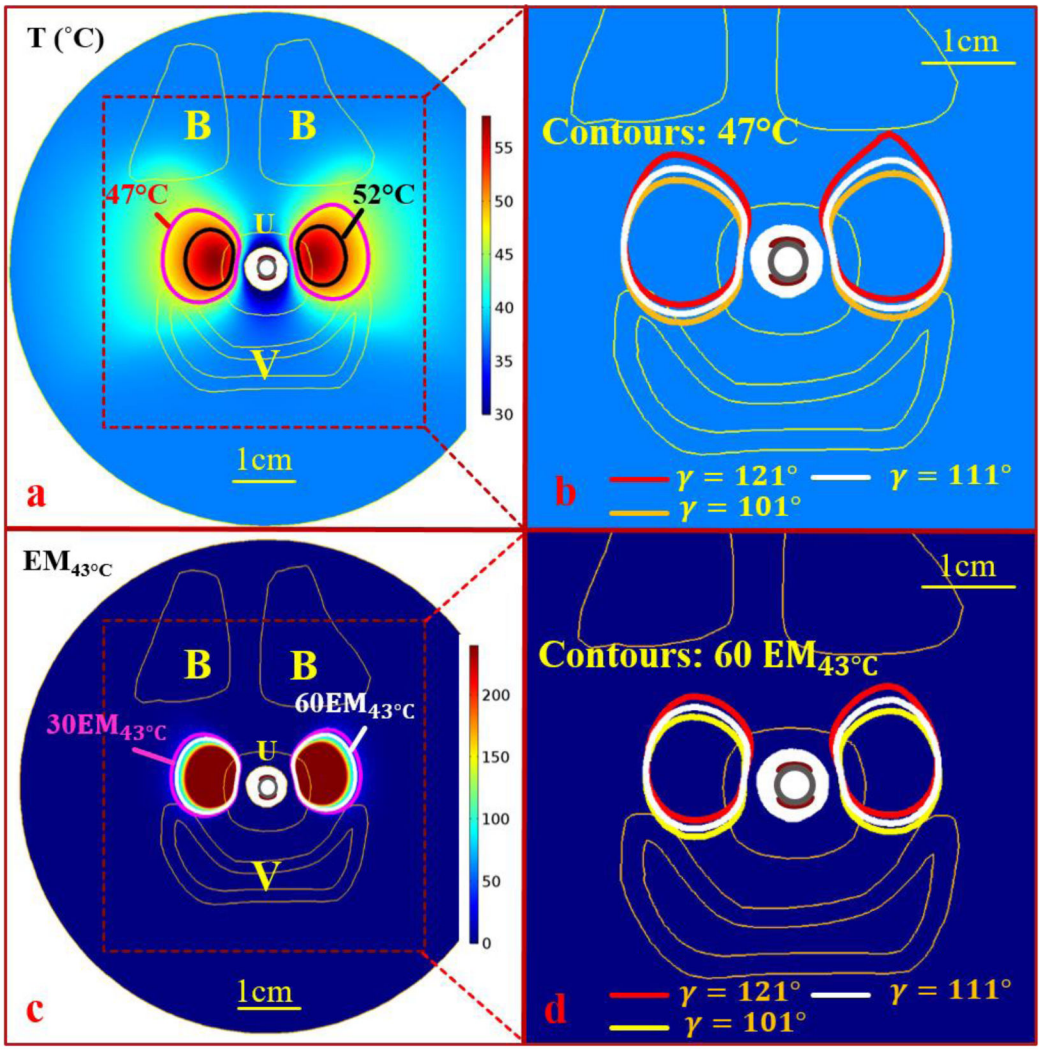

Fig. 6.

Maximum temperature and thermal dose distributions for 3 min sonication of 8.8 W/cm^2 using the dual-sectored tubular ultrasound applicator, across the central axial plane at the mid-urethra level, on Model I representing an “H” shaped vagina: (a-b) Temperature distribution with 111°(a) lower inactive sections and an overlay of 47°C contours with 101°-121° inactive section (c-d) Corresponding thermal doses with 111° lower inactive sections (c) and an overlay of 60 $EM_{43°C}$ contours with 101°-121° lower inactive section. Temperature lower than 30°C and thermal dose over 240 $EM_{43°C}$ were thresholded for display purposes. B, U, and V represent the pubic bones, the urethra, the vagina respectively

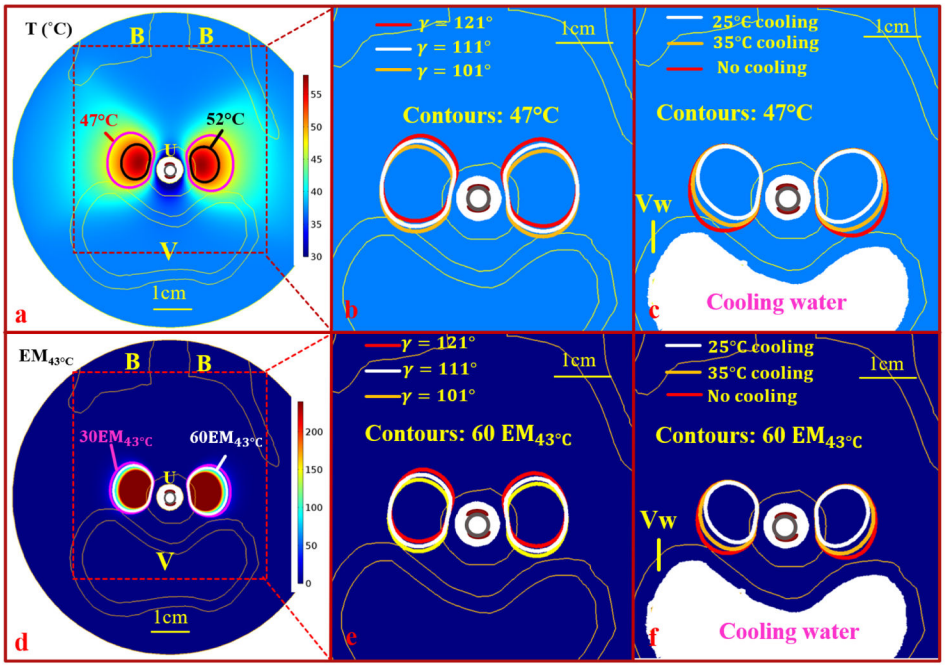

Fig.7.

Maximum temperature and thermal dose distributions for 3 min sonication of 8.8 W/cm^2 using the dual-sectored tubular ultrasound applicator, across the central axial plane at the mid-urethra level, on Model II representing a flattened shape vagina: (a-c) Temperature distribution with 111° lower inactive section, an overlay of 47°C contours with 101-121° inactive sections (b) and an overlay of 47°C with 101° inactive sector and different conditions of endovaginal cooling ((c): no cooling, 25°C and 35°C); (d-f) corresponding thermal doses with 111° lower inactive section (d), an overlay of 60 $EM_{43°C}$ contours with 101-121° inactive sections (e) and an overlay of 60 EM43°C contours with different conditions of endovaginal cooling ((f): no cooling, 25°C and 35°C). Temperature lower than 30°C and thermal dose over 240 $EM_{43°C}$ were thresholded for display purposes. B, U, V and Vw represent the pubic bones, the urethra, the vagina and the outer vaginal wall respectively.

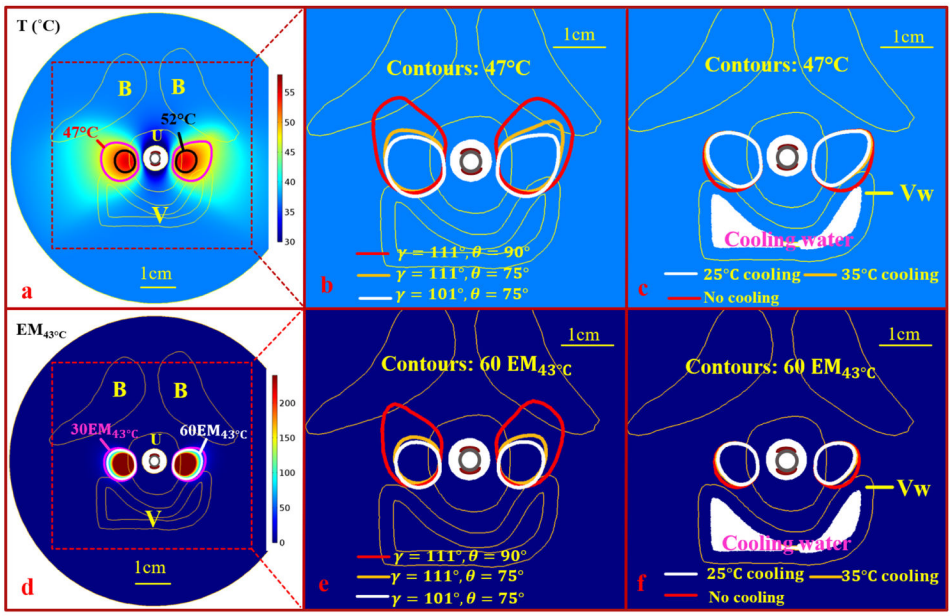

Fig.8.

Maximum temperature and thermal dose distributions for 2 min sonication of 10.2 W/cm^2 using the dual-sectored tubular ultrasound applicator, across the central axial plane at the mid-urethra level, on Model III representing clinically challenging case with very limited retropubic space: (a-c) Temperature distribution with 101° lower inactive section; an overlay of 47°C contours with 101-111° lower inactive sections and 75-90° active sectors (b); and an overlay of 47°C with 101° lower inactive sector and different conditions of endovaginal cooling ((c): no cooling, 25°C and 35°C); (d-f) corresponding thermal doses with 101° lower inactive section (d), an overlay of 60 $EM_{43°C}$ contours with 101-111° inactive sections and 75°-90° active sectors(e), and an overlay of 60 $EM_{43°C}$ contours with different conditions of endovaginal cooling((f): no cooling, 25°C and 35°C). Temperature lower than 30°C and thermal dose over 240 $EM_{43°C}$ were thresholded for display purposes. B, U, V and Vw represent the pubic bones, the urethra, the vagina and the outer vaginal wall respectively.

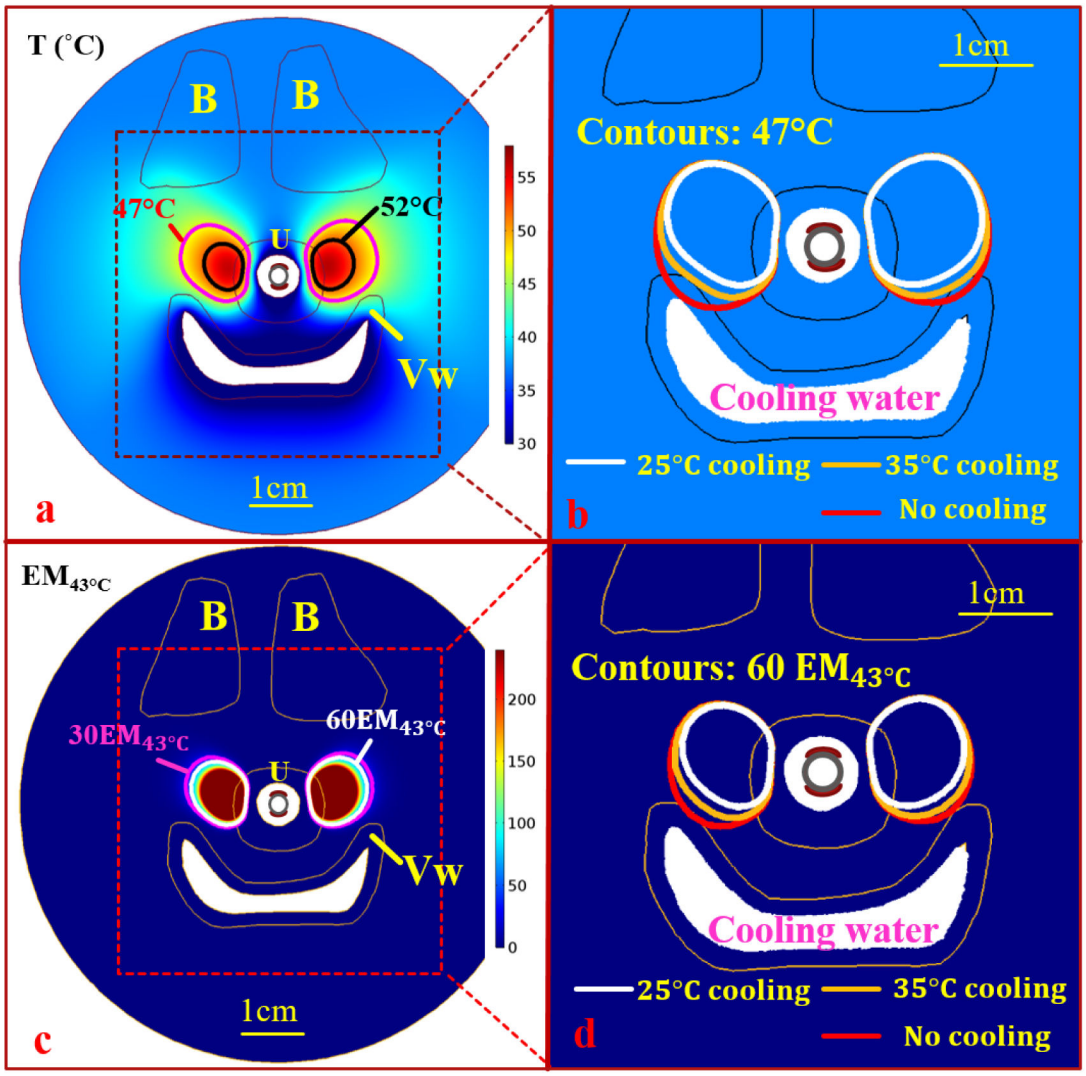

Fig.9.

The temperature (a and b) and thermal dose (c and d) distribution of the central axial plane aligned with the applicator of Model I after 3 mins treatment (8.8 W/cm^2) with 25°C endovaginal cooling (a and c), and overlays of 47°C temperature (b) and 60 $EM_{43°C}$ thermal dose contours (d) : endovaginal cooling could further protect the vagina from heating. Bl, B, U, Vw represent the bladder, the pubic bones, the urethra and vaginal wall respectively.

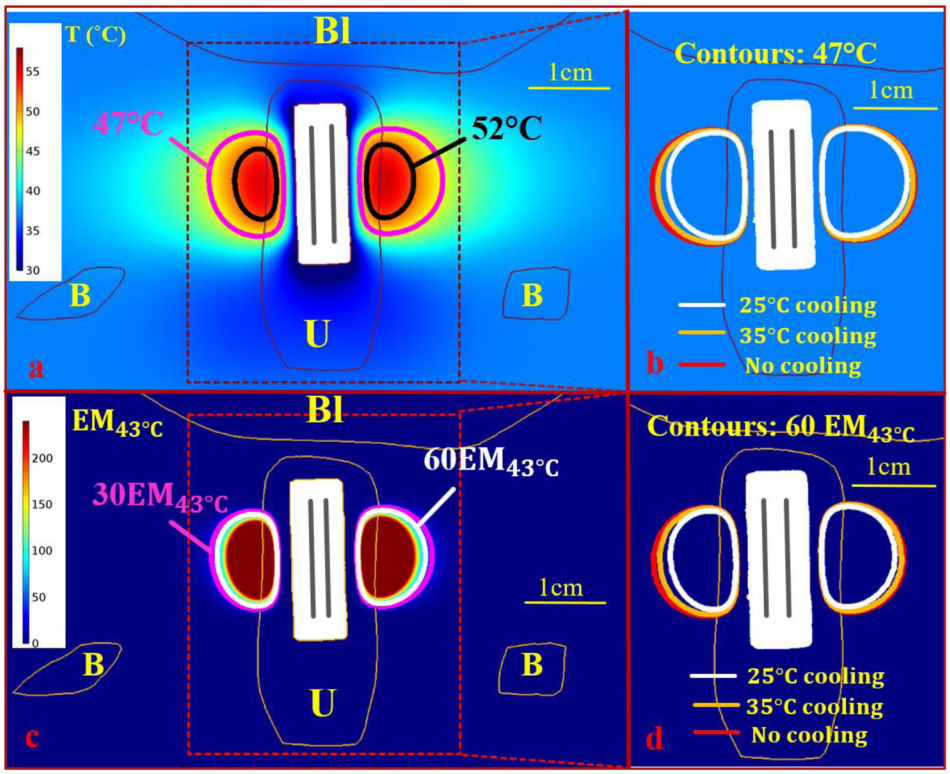

Fig.10.

The temperature (a and b) and thermal dose (c and d) distribution of the central coronal plane aligned with the applicator of Model I after 3 mins treatment with 25°C endovaginal cooling (a and c), overlays of 47°C temperature (b) and 60 $EM_{43°C}$ thermal dose contours (d) : a clear reduction of penetration depth and slight reduction of length with endovaginal cooling. Bl, B, U represent the bladder, the pubic bones and the urethra respectively.

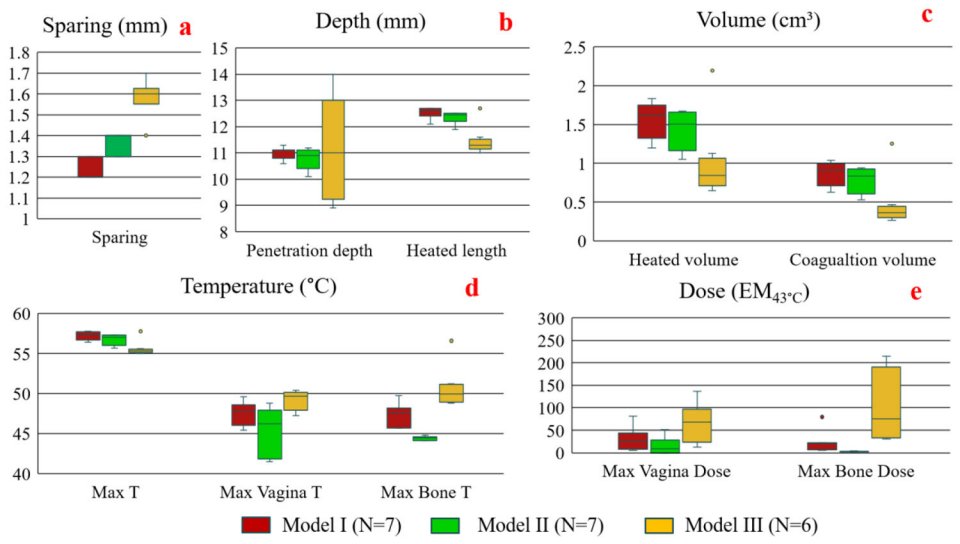

Fig.11.

Summary of urethral sparing (a), penetration depth & heated length (b), heated and coagulation volume (c), target temperature (d) and dose (e) obtained on simulation models I, II and III (Tables 3-5). Data are shown as box plots with median, 25% and 75% ranges, and outliers. N is the total numbers of simulations on each model. For visualization purpose, the outlier point of maximum bone dose (6422.7 $EM_{43°C}$, Table 5) on Model III was not shown in (e).

Table 1

Acoustic and thermal physical properties of the generic and 3D anatomical models [42,45,46]

Tissue Properties	Unit	Generic tissue	Bone[c]	Bladder	Urethra	Vagina
Density	Kg/m^3	1050	1821	1132	1102	1088
Specific heat	J/kg/K	3639	1244	3544	3306	3655
Perfusion[a]	$Kg/m^3/s$	2	0	0.1	3.66	1.88
Thermal conductivity	W/m/K	0.51	0.3	0.51	0.46	0.54
Acoustic Attenuation[b]	Np/m	6.5*f	54.53*f	5.7*f	7.02*f	5.74*f

[a] Perfusion would be reduced to 0 over 300 $EM_{43°C}$ [41]

[b] The working frequency of the applicator is 6.5MHz (f=6.5).

[c] 65% of acoustic energy incident at the bone surface was assumed to be transmitted into the bone[28].

Table 2

Summary of thermal simulation parameters on patient specific models: total elements, degrees of freedom and average simulation time

Model #	Total # of simulations	Active sector angles	Transducer intensities & durations	Total elements	Total degrees of freedom	Average running time(hour/min/sec)
I	7	90°	8.8 W/cm^2, 3 min	2.50 x 10^6	27.2 million (no cooling) 26.3 million (vaginal cooling)	8 hours, 0 min, 18 sec 7 hours, 44 min, 56 sec
II	7	90°	8.8 W/cm^2, 3 min	2.45 x 10^6	26.6 million (no cooling) 24.0 million (vaginal cooling)	8hours, 34 min, 5 sec 7 hours, 18 min, 8 sec
III	6	75°,90°	8.8-10.2 W/cm^2, 2-3 min 10.2 W/cm^2, 2 min	2.48 x 10^6	26.8 million (no cooling) 24.8 million (vaginal cooling)	7 hours, 23 min, 20 sec 6 hours 35 min, 49 sec

Table 3

Summary of thermal simulation on Model I

Metric	Inactive γ=121° No vaginal cooling	Inactive γ=111° No vaginal cooling	Inactive γ=101° No vaginal cooling	Inactive γ=111° 35°C vaginal cooling	Inactive γ=101° 35°C vaginal cooling	Inactive γ=111° 25°C vaginal cooling	Inactive γ=101° 25°C vaginal cooling
Inactive β	59°	69°	79°	69°	79°	69°	79°
Urethra sparing	1.2 mm	1.2 mm	1.2 mm	1.2 mm	1.2 mm	1.3 mm	1.3 mm
Penetration depth[a]	11.3 mm	11.1 mm	11.1 mm	11.1 mm	10.9 mm	10.8 mm	10.6 mm
Heated length[b]	12.7 mm	12.7 mm	12.6 mm	12.6 mm	12.5 mm	12.1 mm	12.0 mm
Heated volume (>60 $EM_{43°C}$)	1.833 cm^3	1.746 cm^3	1.700 cm^3	1.614 cm^3 (−7.6%)[c]	1.521 cm^3 (−10.5%)[c]	1.323 cm^3 (−24.2%)[c]	1.196 cm^3 (−29.6%)[c]
Coagulated volume (>240 $EM_{43°C}$)	1.035 cm^3	0.993 cm^3	0.969 cm^3	0.911 cm^3 (−8.3%)[c]	0.856 cm^3 (−11.6%)[c]	0.709 cm^3 (−28.6%)[c]	0.629 cm^3 (−35.1%)[c]
Max T	57.8°C	57.7°C	57.6°C	57.4°C	57.3°C	56.7°C	56.4°C
Max Vagina T	47.7°C	48.6°C	49.6°C	47.8°C	48.5°C	45.4°C	46.0°C
Max Vagina Dose	25.2 $EM_{43°C}$	43.8 $EM_{43°C}$	81.1 $EM_{43°C}$	26.3 $EM_{43°C}$	40.4 $EM_{43°C}$	5.1 $EM_{43°C}$	7.5 $EM_{43°C}$
Max Bone T	49.7°C	47.7°C	45.7°C	47.6°C	45.7°C	47.5°C	45.5°C
Max Bone Dose	79.4 $EM_{43°C}$	22.4 $EM_{43°C}$	6.4 $EM_{43°C}$	22.1 $EM_{43°C}$	6.3 $EM_{43°C}$	21.1 $EM_{43°C}$	6.0 $EM_{43°C}$
Coverage angles (>60 $_{43°C}$)	73.4°	72.6°	72.1°	71.1°	70.6°	67.0°	65.7°

[a] indicates the maximum penetration (>60 $EM_{43°C}$) in radial direction

[b] indicates the maximum length of heated zone (>60 $EM_{43°C}$) along the applicator

[c] denotes the heated volume reduction compared to the same applicator configurations without vaginal cooling

Table 4

Summary of thermal simulation on Model II

Metric	Inactive γ=121° No vaginal cooling	Inactive γ=111° No vaginal cooling	Inactive γ=101° No vaginal cooling	Inactive γ=111° 35°C vaginal cooling	Inactive γ=101° 35°C vaginal cooling	Inactive γ=111° 25°C vaginal cooling	Inactive γ=101° 25°C vaginal cooling
Inactive β	59°	69°	79°	69°	79°	69°	79°
Urethral sparing	1.3 mm	1.3 mm	1.3 mm	1.4 mm	1.4 mm	1.4 mm	1.4 mm
Penetration depth[a]	11.2 mm	11.1 mm	11.1 mm	10.9 mm	10.8 mm	10.4 mm	10.1 mm
Heated length[b]	12.5 mm	12.5 mm	12.5 mm	12.4 mm	12.3 mm	11.9 mm	11.8 mm
Heated volume (>60 $EM_{43°C}$)	1.674 cm^3	1.655 cm^3	1.632 cm^3	1.506 cm^3 (−9.0%)[c]	1.432 cm^3 (−12.3%)[c]	1.165 cm^3 (−29.6%)[c]	1.054 cm^3 (−35.4%)[c]
Coagulated volume (>240 $EM_{43°C}$)	0.940 cm^3	0.928 cm^3	0.914 cm^3	0.836 cm^3 (−10.0%)[c]	0.790 cm^3 (−13.6%)[c]	0.603 cm^3 (−35.0%)[c]	0.531 cm^3 (−41.9%)[c]
Max T	57.3°C	57.3°C	57.3°C	57.0°C	56.9°C	56.0°C	55.7°C
Max Vagina T	46.8°C	47.9°C	48.8°C	45.7°C	46.2°C	41.5°C	41.8°C
Max Vagina Dose	14.3 $EM_{43°C}$	29.0 $EM_{43°C}$	51.2 $EM_{43°C}$	6.8 $EM_{43°C}$	9.4 $EM_{43°C}$	0.09 $EM_{43°C}$	0.14 $EM_{43°C}$
Max Bone T	44.8°C	44.5°C	44.1°C	44.5°C	44.1°C	44.4°C	44.0°C
Max Bone Dose	3.9 $EM_{43°C}$	3.2 $EM_{43°C}$	2.3 $EM_{43°C}$	3.1 $EM_{43°C}$	2.2 $EM_{43°C}$	2.9 $EM_{43°C}$	2.1 $EM_{43°C}$
Coverage angles (>60 $EM_{43°C}$)	71.7°	71.7°	71.4°	70.0°	69.3°	64.2°	62.6°

[a] indicates the maximum penetration (>60 $EM_{43°C}$) in radial direction

[b] indicates the maximum length of heated zone (>60 $EM_{43°C}$) along the applicator

[c] denotes the heated volume reduction compared to the same applicator configurations without vaginal cooling

Table 5

Summary of thermal simulation on Model III

Metric	Inactive γ=111° No vaginal cooling	Inactive γ=111° No vaginal cooling	Inactive γ=111° No vaginal cooling	Inactive γ=101° No vaginal cooling	Inactive γ=101° 35°C vaginal cooling	Inactive γ=101° 25°C vaginal cooling
Inactive β	69°	99°	99°	109°	109°	109°
Active θ	90°	75°	75°	75°	75°	75°
Acoustic intensities	8.8 W/cm^2	8.8 W/cm^2	10.2 W/cm^2	10.2 W/cm^2	10.2 W/cm^2	10.2 W/cm^2
Durations	3min	3min	2min	2min	2min	2min
Urethral sparing	1.4 mm	1.7 mm	1.6 mm	1.6 mm	1.6 mm	1.6 mm
Penetration depth[a]	14.0 mm	13.2 mm	12.4 mm	9.6 mm	9.1 mm	8.9 mm
Heated length[b]	12.7 mm	11.6 mm	11.3 mm	11.3 mm	11.1 mm	11.0 mm
Heated volume (>60 $EM_{43°C}$)	2.192 cm^3	1.129 cm^3	0.876 cm^3	0.805 cm^3	0.680 cm^3 (−15.5%)[c]	0.645 cm^3 (−19.9%)[c]
Coagulated volume (>240 $EM_{43°C}$)	1.256 cm^3	0.469 cm^3	0.370 cm^3	0.348 cm^3	0.286 cm^3 (−17.8%)[c]	0.267 cm^3 (−23.3%)[c]
Max T	57.8°C	55.0°C	55.6°C	55.5°C	55.2°C	55.1°C
Max Vagina T	50.4°C	49.9°C	49.4°C	50.2°C	47.4°C	47.2°C
Max Vagina Dose	137.1 $EM_{43°C}$	100.9 $EM_{43°C}$	50.8 $EM_{43°C}$	85.2 $EM_{43°C}$	14.2 $EM_{43°C}$	12.2 $EM_{43°C}$
Max Bone T	56.6°C	51.2°C	50.9°C	49.0°C	48.9°C	48.8°C
Max Bone Dose	6422.7 $EM_{43°C}$	215.2 $EM_{43°C}$	116.9 $EM_{43°C}$	34.8 $EM_{43°C}$	33.0 $EM_{43°C}$	30.5 $EM_{43°C}$
Coverage angles (>60 $EM_{43°C}$)	75.5°	56.7°	52.6°	52.0°	50.2°	50.0°

[a] indicates the maximum penetration (>60 $EM_{43°C}$) in radial direction

[b] indicates the maximum length of heated zone (>60 $EM_{43°C}$) along the applicator

[c] denotes the heated volume reduction compared to the same applicator configurations without vaginal cooling